

2008

# A Study of the Air-Side Heat Transfer and Pressure Drop Characteristics of Tube-Fin 'No-Frost' Evaporators

Jader R. Barbosa

*Federal University of Santa Catarina*

Claudio Melo

*Federal University of Santa Catarina*

Christian J. L. Hermes

*Federal University of Santa Catarina*

Follow this and additional works at: <http://docs.lib.purdue.edu/iracc>

---

Barbosa, Jader R.; Melo, Claudio; and Hermes, Christian J. L., "A Study of the Air-Side Heat Transfer and Pressure Drop Characteristics of Tube-Fin 'No-Frost' Evaporators" (2008). *International Refrigeration and Air Conditioning Conference*. Paper 874. <http://docs.lib.purdue.edu/iracc/874>

This document has been made available through Purdue e-Pubs, a service of the Purdue University Libraries. Please contact [epubs@purdue.edu](mailto:epubs@purdue.edu) for additional information.

Complete proceedings may be acquired in print and on CD-ROM directly from the Ray W. Herrick Laboratories at <https://engineering.purdue.edu/Herrick/Events/orderlit.html>

## A Study of the Air-Side Heat Transfer and Pressure Drop Characteristics of Tube-Fin 'No-Frost' Evaporators

Jader R BARBOSA Jr. \*, Cláudio MELO, Christian J L HERMES

Federal University of Santa Catarina,  
Department of Mechanical Engineering,  
Florianópolis, SC, 88040900, Brazil

\*Corresponding Author

Phone/Fax: ++ 55 48 3234 5166, e-mail: jrb@polo.ufsc.br

### ABSTRACT

A study is presented on the influence of air flow rate and surface geometry on the thermal-hydraulic performance of commercial tube-fin 'no-frost' evaporators. A specially constructed wind-tunnel calorimeter was used in the experiments from which data on the overall thermal conductance, pressure drop, Colburn  $j$ -factor and Darcy friction factor,  $f$ , were extracted. Eight different evaporator samples with distinct geometric characteristics, such as number of tube rows, number of fins and fin pitch were tested. Semi-empirical correlations for  $j$  and  $f$  are proposed in terms of the air-side Reynolds number and the finning factor. A discussion is presented on the performance of the evaporators with respect to specific criteria such as the pumping power as a function of heat transfer capacity and the volume of material in each evaporator.

### 1. INTRODUCTION

Compartment cooling in the so-called 'no-frost' refrigerators relies on external forced convection heat transfer to a tube-fin evaporator. Despite the abundant literature on air-side thermal-hydraulic performance of tube-fin heat exchangers, there is a lack of specific experimental data for the class of evaporators used in 'no-frost' household appliances. In relation to more conventional tube-fin heat exchangers, there are several distinguishing aspects of 'no-frost' evaporators which make them unique. Firstly, the geometry of 'no-frost' evaporators is such that the frontal (or face) area is smaller and the evaporator length is larger than more conventional heat exchanger geometries. Thus, in 'no-frost' evaporators, the number of tube rows through which the air flows is considerably larger (see Fig. 1). In addition, to avoid flow obstruction due to frost formation on the air-side heat transfer surface, fin spacing may be non-uniform along the coil and is significantly larger ( $\sim 1/2$  fpi) than those found in conventional tube-fin exchangers ( $\sim 20$  fpi). Also, the range of air flow rates in 'no-frost' evaporators tend to be lower than in conventional tube-fin heat exchangers (typically lower than  $50 \text{ m}^3/\text{h}$ ).

Karatas *et al.* (1996) carried out an experimental study of the air-side heat transfer and pressure drop in 'no-frost' evaporators. They tested four evaporators and assessed the effect of non-uniformities in the temperature and velocity distributions of the inlet air flow. Although the number of fins (and hence the fin spacing and finning factor) was different for each evaporator, their basic characteristics (tube pitches, number of tube rows, number of tubes per row, face dimensions) were kept constant. Correlations were proposed for the Colburn  $j$ -factor and for the friction factor as a function of the air-side Reynolds number, the Prandtl number and the finning factor. They concluded that the heat transfer correlation was equally valid for the non-uniform flow cases (typical operating condition of Combi refrigerators, where air is drawn from both the freezer and fresh-food compartments) if mass flow averaged values of temperature and velocity were used at the evaporator inlet.

Lee *et al.* (2002) investigated experimentally the behavior of the air-side heat transfer coefficient for the same evaporator configuration, but with three different fin geometries (discrete flat plate fins, continuous flat plate fins

and spine fins). Despite the lower evaporator length and smaller heat transfer area, the spine finned tube evaporator exhibited the best thermal-hydraulic performance under ‘dry’ conditions (no condensate or frost formation). The authors put forward correlations for the Nusselt number for the three evaporators.

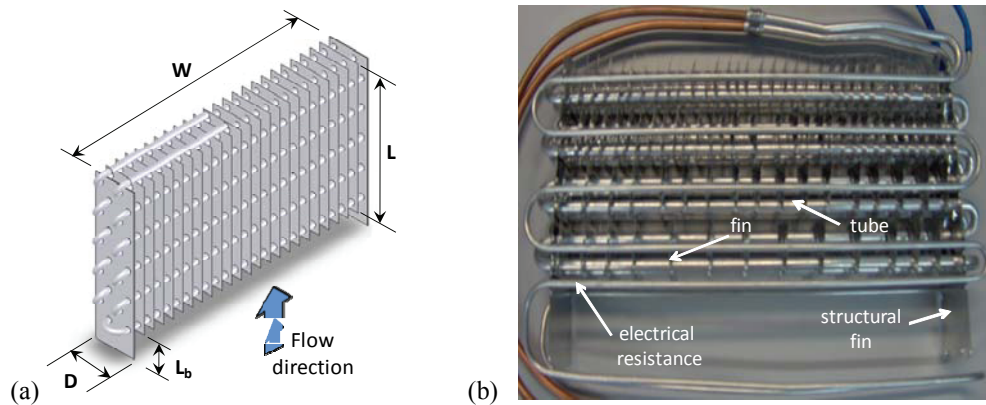


Figure 1: (a) A typical ‘no-frost’ evaporator, (b) an evaporator used in the study.

It is important to note that the studies of Karatas et al. (1996) and Lee et al. (2002) kept the number of tube rows fixed (13 and 10 rows, respectively), neglecting the importance of such design parameter in the heat exchanger performance. The assessment of the effect of the number of tube rows on the evaporator thermal-hydraulic performance is, therefore, the main focus of the present study. Thus, in this paper, a systematic investigation of the influence of several geometric parameters (e.g., number of tube rows, fin pitch, number of fins) and air flow rate on the air-side thermal-hydraulic performance of tube-fin ‘no-frost’ evaporators under ‘dry’ conditions is reported. Eight evaporator samples were evaluated and the variation of geometric parameters between the samples resulted in distinct values of evaporator length, heat transfer surface area and volume of material (mass of aluminum). A purpose-built wind-tunnel calorimeter was used in the experiments from which overall thermal conductance, pressure drop, Colburn  $j$ -factor and Darcy friction factor,  $f$ , data were extracted. The experimental data expressed in terms of  $j$  and  $f$  were reproduced by empirical correlations within  $\pm 7\%$  error bands.

## 2. EXPERIMENTAL WORK

### 2.1 Facility and Equipment

The wind tunnel was designed according to ANSI/ASHRAE Standards 37 (1987), 41.2 (1988) and 51 (1999). The facility was constructed from a double layer of ordinary steel plates. In between the plates, a 100 mm thick layer of glass wool was inserted to provide thermal insulation. The test section dimensions are illustrated in Fig. 2. Screens are employed to make the flow uniform in the inlet and exit sections and also upstream of the air flow nozzles. In this region, the height of the test section was increased to accommodate the nozzle array used for measuring the air flow rate.

The following components comprise the wind tunnel air-side instrumentation: a 51-W speed controlled fan, a 400-W (max.) PID controlled electrical heater for air inlet temperature setting, a set of 5 aluminum nozzles with diameters ranging from 0.75” to 1.25”, and 2 differential pressure transducers to measure the air pressure drop across the evaporator and the nozzles. The evaporator pressure drop is measured by mounting perforated hoses (spacing between adjacent holes of 50 mm) on two grooves machined on the bottom wall of the test section (one upstream and the other downstream of the evaporator). The grooves are perpendicular to the main flow direction and their depth is such that the pressure taps are at the same level as the bottom wall. The adjoining surfaces are leveled with silicone glue to avoid disturbing the flow in the vicinity of the pressure taps. One end of each hose is connected to the differential pressure transducer while the other end is sealed. The accuracy of each pressure transducer is  $\pm 0.5\%$  of the full scale ( $\sim 25$  Pa for the evaporator transducer and  $\sim 995$  Pa for the nozzle transducer). Operation limits and design conditions are as follows; air flow rate: min 17 m<sup>3</sup>/h (10 cfm), max 102 m<sup>3</sup>/h (60 cfm), nominal 51 m<sup>3</sup>/h (30 cfm); and heat transfer rate: min 40 W, max 200 W, nominal 120 W. The maximum evaporator dimensions for the test section are: height 250 mm, length 580 mm, width 80 mm.

The main function of the water loop is to circulate water at controlled temperatures and flow rates through the evaporator. The following components make up the water circuit: a 1.58 L/min (max.) speed-controlled rotary pump; a 100°C (max.),  $\pm 0.1$  °C accuracy, thermostatic bath; and a 2.46 L/min (max.), 1.4% full scale accuracy, turbine flow meter. The loop is thermally insulated and T-type immersion thermocouples ( $\pm 0.1$  °C) are placed immediately upstream and downstream of the evaporator. Data acquisition is performed with a PC integrated 40 channel system. This system, in conjunction with a purpose-built control panel, monitors and records pressure, temperature, relative humidity and water flow rate signals.

## 2.2. Procedure

The apparatus is switched on, the inlet water temperature (approximately 32°C in all cases) is set and approximately 10 minutes are required for it to stabilize. The desired air flow rate is adjusted and the inlet air temperature is set (approximately 28°C in all cases). The water flow rate is set to provide roughly a 0.5°C temperature variation between the inlet and outlet the exchanger. Approximately 50 to 80 minutes – depending on the flow rates – are required to reach steady-state. A steady-state criterion based on the average of each measured parameter as a function of time with respect to the standard deviation associated with its readings was adopted. Temperatures, pressures and other signals are recorded and averaged over a time interval of 30 minutes. After data collection for one experimental condition, the flow rates are altered so that a new experimental condition is achieved.

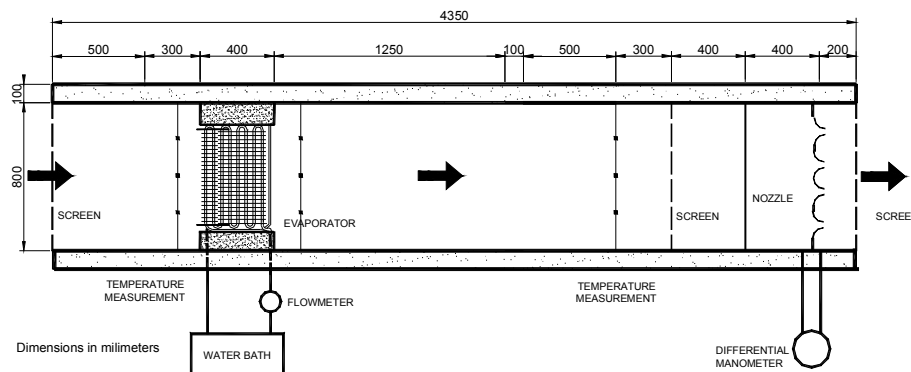


Figure 2: A schematic view of the section of the wind-tunnel.

## 2.3. Evaporator Samples

Eight sample evaporators made from aluminum (both fin and tubes) were tested. The inner and outer diameters of the tubes in all evaporators were 6.6 mm and 7.9 mm, respectively. The number of tubes per row is 2 in all exchangers. A staggered tube array is used in all samples and the transverse and longitudinal tube pitches are 23 mm and 22 mm, respectively. The width,  $W$ , and depth (thickness),  $D$ , in all evaporators are 340 mm and 59 mm. The geometry of the discrete flat fins is such that their height and width are fixed at 35 mm and 59 mm and they are mounted so as to span two consecutive tube rows (for example, in an evaporator with  $N$  tube rows there are  $N/2$  fin rows). The fin thickness is 0.127 mm. As shown in Fig. 1.b, the evaporator coil is assembled on two 1 mm thick structural fins, which also provide support for mounting the electrical resistances for defrosting. The evaporator length,  $L$ , is defined as the distance between the tips of the fins at the inlet and outlet sections. The length of the structural fins is equal to  $L + L_b$  in all evaporators ( $L_b = 55$  mm). The number of tube rows, the evaporator length, the number of fins per meter per row, the surface area of the fins and of the tubes, the finning factor and the amount of material (evaporator mass) may vary between the samples and their values are summarized in Table 1. The tests were conducted with the defrosting electrical resistances mounted on the heat exchangers.

## 3. DATA REGRESSION

### 3.1 Heat Transfer

The heat transfer rate from the exchanger is taken as the arithmetic mean of the air and water loops heat transfer rates (Eq. 1). In all experimental runs, the difference between  $\dot{Q}_a$  and  $\dot{Q}_w$  was never higher than 5%.

$$\dot{Q} = \frac{1}{2}(\dot{Q}_a + \dot{Q}_w) = \frac{1}{2}[\dot{m}_a c_{P,a} (T_{a,out} - T_{a,in}) + \dot{m}_w c_{P,w} (T_{w,in} - T_{w,out})] \quad (1)$$

Table 1: Geometric parameters of evaporator samples

Evaporator sample	Tube rows	Length [mm]	Fins	Area [m <sup>2</sup> ]	Finning factor	Fin density [cm <sup>-1</sup> ]	Mass [g]
#1	4	74	61	fins: 0.20 tube: 0.07 total: 0.27	3.86	1 <sup>st</sup> fin row: 0.79 2 <sup>nd</sup> fin row: 1.00	380.6
#2	6	112	128	fins: 0.41 tube: 0.10 total: 0.51	5.10	1 <sup>st</sup> fin row: 0.79 2 <sup>nd</sup> fin row: 1.00 3 <sup>rd</sup> fin row: 1.97	496.4
#3	8	151	194	fins: 0.61 tube: 0.14 total: 0.75	5.36	1 <sup>st</sup> fin row: 0.79 2 <sup>nd</sup> fin row: 1.00 3 <sup>rd</sup> fin row: 1.97 4 <sup>th</sup> fin row: 1.94	607.1
#4	10	189	129	fins: 0.42 tube: 0.17 total: 0.59	3.47	1 <sup>st</sup> fin row: 0.79 2 <sup>nd</sup> fin row: 1.00 3 <sup>rd</sup> fin row: 1.00 4 <sup>th</sup> fin row: 0.50 5 <sup>th</sup> fin row: 0.50	677.3
#5	8	151	95	fins: 0.31 tube: 0.14 total: 0.55	3.93	1 <sup>st</sup> fin row: 0.41 2 <sup>nd</sup> fin row: 0.50 3 <sup>rd</sup> fin row: 0.91 4 <sup>th</sup> fin row: 0.97	560.0
#6	10	189	261	fins: 0.82 tube: 0.17 total: 0.99	5.82	1 <sup>st</sup> fin row: 0.79 2 <sup>nd</sup> fin row: 1.00 3 <sup>rd</sup> fin row: 1.97 4 <sup>th</sup> fin row: 1.94 5 <sup>th</sup> fin row: 1.97	776.6
#7	4	74	31	fins: 0.11 tube: 0.07 total: 0.18	2.57	1 <sup>st</sup> fin row: 0.41 2 <sup>nd</sup> fin row: 0.50	350.3
#8	6	112	65	fins: 0.22 tube: 0.10 total: 0.32	3.20	1 <sup>st</sup> fin row: 0.41 2 <sup>nd</sup> fin row: 0.50 3 <sup>rd</sup> fin row: 1.00	503.3

The overall thermal conductance is calculated using the Log-Mean Temperature Difference approach (Kays and London, 1994), as follows

$$UA = \frac{\dot{Q}}{(F\Delta T_{lm})} = \frac{\dot{Q} \ln[(T_w - T_{a,in})/(T_w - T_{a,out})]}{(T_w - T_{a,in}) - (T_w - T_{a,out})} \quad (2)$$

where  $F=1$  due to the negligible water temperature drop across the exchanger. The air-side heat transfer coefficient is calculated neglecting the thermal resistance of the tube wall,

$$h_o = \left\{ \left( \frac{\eta_o A_o}{UA} \right) - \left( \frac{\eta_o A_o}{A_i h_i} \right) \right\}^{-1} \quad (3)$$

where the water-side heat transfer coefficient,  $h_i$ , was estimated using the Gnielinski correlation (Incropera and DeWitt, 1990). The parameters related to the finned surface geometry are given by (Lee et al., 2002)

$$\eta_o A_o = A_{to} + \eta_{fin} A_{fin} \quad (4)$$

$$\eta_{fin} = \tanh(\phi m r_o) / \phi m r_o \quad (5)$$

$$m = \sqrt{2h_o / k_{fin} t_{fin}} \quad (6)$$

$$\phi = (r_{eq}/r_o - 1) [1 + 0.35 \ln(r_{eq}/r_o)] \quad (7)$$

$$r_{eq}/r_o = 1.28 X_M / r_o \sqrt{X_L / X_M} - 0.3 \quad (\text{Staggered tube array}) \quad (8)$$

$$X_M = P_t / 2 \quad (9)$$

$$X_L = \sqrt{(P_t/2)^2 + (P_t/2)^2} \quad (10)$$

The Colburn  $j$ -factor is calculated from

$$j = \frac{h_o}{G_{a,\max} C_{P,a}} \text{Pr}_a^{2/3} \quad (11)$$

$$G_{a,\max} = \dot{m}_a / A_{\min} \quad (12)$$

where  $A_{\min}$  is the minimum flow cross-section area on the air side calculated from

$$A_{\min} = DW - N_{fin}Dt - 2d_{to}W + 2d_{to}t \quad (13)$$

### 3.2 Pressure Drop

Based on the measured air-side pressure drop, the friction factor is calculated as follows (Kays and London, 1994),

$$f = \frac{A_{\min}}{A_o} \frac{\rho_a}{\rho_{a,in}} \left\{ \frac{2\Delta p_a \rho_{a,in}}{G_{a,\max}^2} - \left( \frac{\rho_{a,in}}{\rho_{a,out}} - 1 \right) \left( 1 + \frac{A_{\min}^2}{A_f^2} \right) \right\} \quad (14)$$

where  $\rho_a$  is the average air density evaluated at the average temperature between the inlet and outlet.

A series of repeatability tests were performed and it was found that pressure drop, friction factors, overall thermal conductance and  $j$ -factors are reproducible within the uncertainty levels corresponding to  $\pm 5\%$ ,  $\pm 8\%$ ,  $\pm 8\%$  and  $\pm 9\%$ , respectively.

## 4. RESULTS AND DISCUSSION

Air-side pressure drop as a function of air flow rate is presented in Fig. 3. The expected behavior of increasing pressure drop with increasing flow rate is observed. The effect of fin number on pressure drop is quite pronounced but, as will be seen, this is less than the effect of fin number on thermal conductance. For example, evaporator #4 exhibits a somewhat higher pressure drop than evaporator #3, even though the former has fewer fins (and also a lower total heat transfer surface). In this case, the reduction in pressure drop due to the lower number of fins in sample #4 is offset by an increase in pressure drop due to the greater number of tube rows in sample #4 compared to sample #3. The more distinct influence of the number of tube rows on pressure drop can also be observed by comparing the pressure drop curves for samples #2 and #4, which have almost the same number of fins, but a different number of tube rows.

Figure 4 presents the overall thermal conductance of the eight evaporator samples as a function of the air flow pumping power, given by the product of the air volume flow rate and the air-side pressure drop. As expected,  $UA$  increases with air flow rate and pumping power in all cases. The total number of fins seems to be the most important parameter controlling the magnitude of  $UA$ , since the lowest conductance at a give flow rate is that of sample #7 and this increases progressively as the total number of fins, and hence the heat transfer surface area, increases (sample #6 exhibits the highest conductance at all flow rates). The number of tube rows also contributes for an increase in  $UA$ , but the increase in surface area due to a larger number of tube rows is in some cases overcome by that associated with more fins distributed over a lower number of tube rows (as in the cases of evaporators #2 to #5).

Curves of Colburn  $j$ -factor and friction factor as a function of the air-side Reynolds number are presented in Figures 5 and 6, respectively. The air-side Reynolds number is calculated based on the maximum air mass flux through the evaporator,

$$\text{Re}_a = D_h G_{a,\max} / \mu_a \quad (15)$$

where  $\mu_a$  is the average air viscosity evaluated at the average temperature between the inlet and outlet. The expected behavior of decreasing  $j$  and  $f$  with Reynolds number is observed. The shift between the curves characterizes the effect of fin number, fin distribution and evaporator length on heat transfer and pressure drop.

Empirical correlations for the  $j$ -factor and for the friction factor were devised based on the whole experimental data set and are presented below. These include the air-side Reynolds number, the finning factor and the number of fin rows as follows,

$$j = 0.5685 Re_a^{-0.4446} \epsilon^{-0.3824} \tag{16}$$

$$f = 5.9051 Re_a^{-0.2973} \epsilon^{-0.7487} (N/2)^{-0.4379} \tag{17}$$

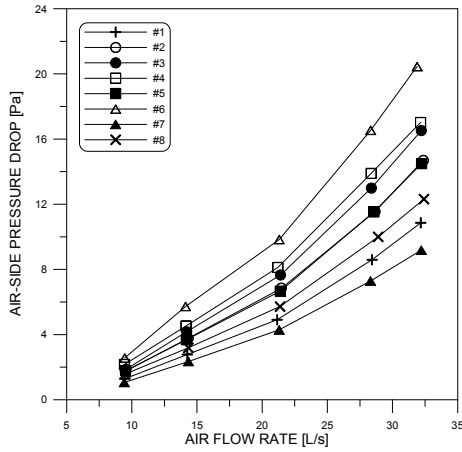


Figure 3: Air-side pressure drop.

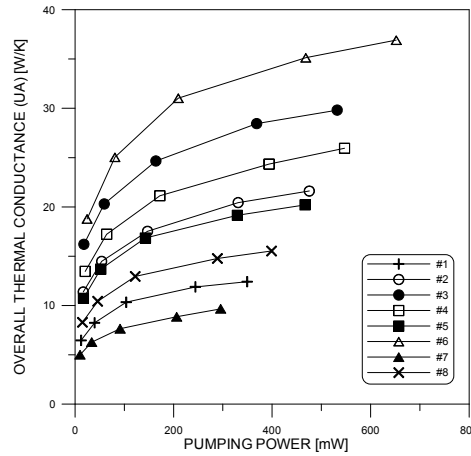


Figure 4: Overall thermal conductance.

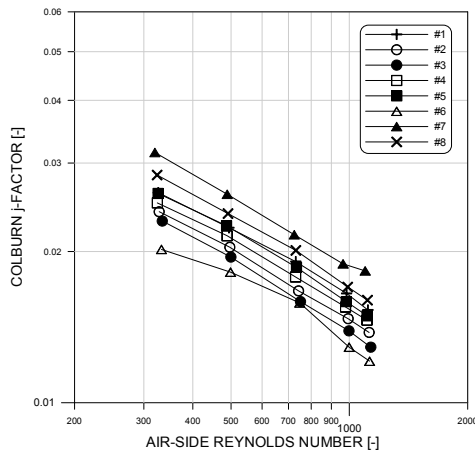


Figure 5: Colburn  $j$ -factor as a function of Reynolds number.

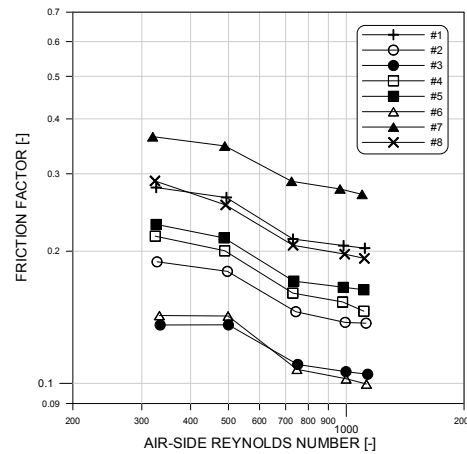


Figure 6: Friction factor as a function of Reynolds number.

The form of the correlations for  $j$  and  $f$  reflects the experimental observations that the number of tube rows (and hence of fin rows) exerts a stronger influence on pressure drop than on the overall heat conductance. For this reason, this parameter was considered only in the  $f$  correlation. The constants were determined through minimization of the RMS error given by Eq. (18) using a Quasi-Newton method.

$$RMS = \sqrt{\frac{1}{N} \sum_i \left( \frac{g_{cal,i} - g_{exp,i}}{g_{exp,i}} \right)^2} \tag{18}$$

where  $g$  can be either  $j$  or  $f$ . Figures 7 and 8 show comparisons between calculated and experimental  $j$ -factor and friction factors, respectively. As can be seen, the models can predict the experimental data within  $\pm 7\%$  error bands. The correlations are valid for  $320 \leq Re_a \leq 1200$ ,  $2.6 \leq \epsilon \leq 5.8$  and  $2 \leq (N/2) \leq 5$ .

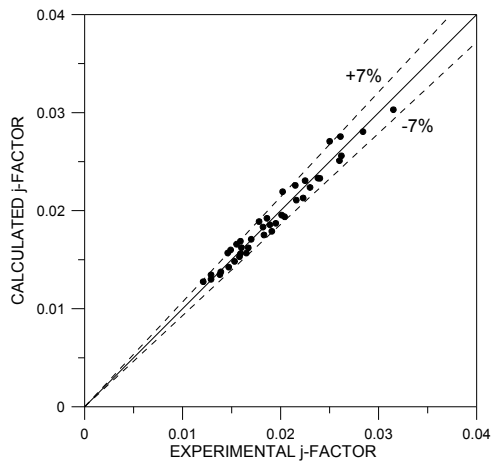


Figure 7: Comparison of calculated and experimental  $j$ -factors.

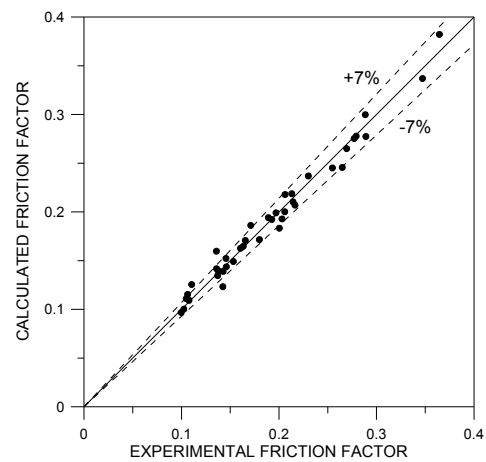


Figure 8: Comparison of calculated and experimental friction factors.

Figure 9 presents a comparison between the performances of each evaporator sample. The pumping power as a function of the heat transfer capacity, as calculated from the empirical correlations, is plotted for each evaporator. At low heat transfer capacities, all evaporators seem capable of providing the desired cooling capacity with a low pumping power. At high heat transfer capacities, on the other hand, the pumping power for the small evaporators becomes prohibitive.

The above information, together with the fact that the mass of aluminum in the evaporator decreases significantly with a decrease in the number of tube rows (as can be seen from Table 1) represents an important aspect to be taken into account in the appliance design and cost assessment. This matter should, however, be regarded as an issue to be dealt with in conjunction with a more thorough analysis considering the mechanism of frost formation and defrosting operations.

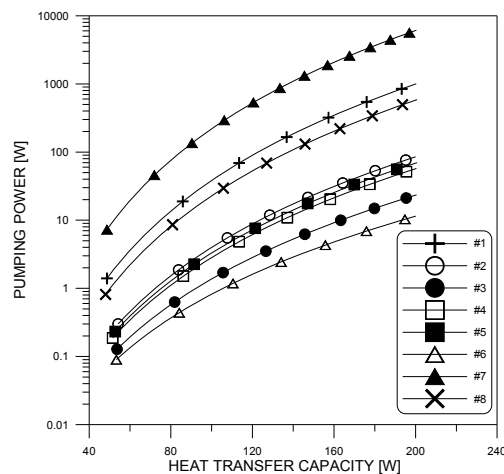


Figure 9. Calculated pumping power as a function of heat transfer capacity.

## 5. CONCLUSIONS

This paper presented experimental data on the thermal-hydraulic performance of evaporators used in 'no-frost' household appliances. An open wind-tunnel test facility specially designed and built for testing this type of evaporator was utilized and data on overall thermal conductance, pressure drop,  $j$  and  $f$  were collected for eight evaporators with different geometric characteristics. It was found that, when using  $j/f$  as a performance evaluation criterion, evaporators with lower length (i.e., fewer tube rows) and lower surface area performed better than some of their counterparts indicating that the last tube rows contribute less effectively to heat transfer, whilst still exert some influence on pressure drop. Moreover, the analysis indicates clearly that cost savings can be achieved by using lighter evaporators with equivalent (in some cases improved) performance characteristics.

## NOMENCLATURE

$A$	area	(m <sup>2</sup> )	<b>Subscripts</b>	
$c_p$	specific heat capacity	(J/kg.K)	$a$	air
$D_h$	hydraulic diameter	(m)	$f$	face
$G$	mass flux	(kg/m <sup>2</sup> .s)	$i$	inner
$h$	heat transfer coefficient	(W/m <sup>2</sup> .K)	$in$	inlet
$k$	thermal conductivity	(W/m.K)	$o$	outer
$\dot{m}$	mass flow rate	(kg/s)	$out$	outlet
$N$	number of tube rows	(-)	$t$	tube
$P_l$	longitudinal tube pitch	(m)	$w$	wall
$P_t$	transverse tube pitch	(m)		
$Pr$	Prandtl number	(-)		
$\dot{Q}$	heat transfer rate	(W)		
$r$	tube radius	(m)		
Re	Reynolds number	(-)		
$t$	thickness	(m)		
$T$	temperature	(°C)		
$UA$	overall thermal conductance	(W/°C)		
$\varepsilon$	finning factor	(-)		
$\eta$	efficiency	(-)		

## REFERENCES

- ANSI/ASHRAE 37, 1988, Methods of Testing for Rating Unitary Air-Conditioning and Heat Pump Equipment, Atlanta, GA.
- ANSI/ASHRAE 41.2, 1987 (RA 92), Standard Methods for Laboratory Airflow Measurement, Atlanta, GA.
- ANSI/ASHRAE 51, 1999, Laboratory Methods of Testing Fans for Aerodynamic Performance Rating, Atlanta, GA.
- Incropera, F.P., DeWitt, D.P., 1990, *Fundamentals of Heat and Mass Transfer*, 3<sup>rd</sup> Ed., Wiley, NY.
- Karatas, H., Dirik, E., Derbentil, T., 1996, An Experimental Study of Air-Side Heat Transfer and Friction Factor Correlations on Domestic Refrigerator Finned-Tube Evaporator Coils, 8th International Refrigeration and Air Conditioning Conference at Purdue, West Lafayette, IN, July 25-28.
- Kays, W.M., London, A.L., 1994, *Compact Heat Exchangers*, 3<sup>rd</sup> Ed., Krieger, Malabar, FL, USA
- Lee, T.-H., Lee, J.-S., Oh, S.-Y., Lee, M.-Y., Lee, K.-S., 2002, Comparison of Air-Side Heat Transfer Coefficients of Several Types of Evaporators of Household Freezer/Refrigerators, 9th International Refrigeration and Air Conditioning Conference at Purdue, West Lafayette, IN, July 16-19.

## ACKNOWLEDGEMENTS

The authors are grateful to Messrs. L.G. Pereira, J. Boeng, R.O. Piucco, A. Berwanger, A.G.U. Souza and G.A. Rodrigues for their valuable support in the experiments and data correlation. Financial support from Whirlpool S.A. is duly acknowledged.